Optical Measurements of Mass Density in a High-Speed, Confined, Gaseous Vortex

GEORGE GYARMATHY*
Brown, Boveri and Company Ltd., Baden, Switzerland

An optical method based on light-deflection mapping has been developed and used to determine the radial variation of fluid density in a high-pressure ratio, high-speed, air vortex that was generated in a 3-in.-diam, 18-in.-long swirl chamber consisting of two symmetric halves. An intense, parallel, thin light beam was transmitted laterally through the vortex at various off-axis positions, and the small light deflections caused by the density field of the vortex were measured. From the variation of the deflection angle over the radius, the radial density profile was numerically calculated by assuming rotational symmetry and solving the resulting integral equation. The density profile of the vortex was determined in two cross sections, at various operating conditions of the chamber. The results show that the core region in which the fluid rotates like a solid body has a very uniform diameter corresponding to about half of the exhaust port diameter. The presence of slight axial density differences, which are related to the meridional flow movements, is clearly shown. The lowest density is found to occur at the vortex axis in the central portion of the chamber. From the density profiles and suitably corrected pressure profiles measured with probes, static temperature profiles were calculated; the temperature exhibits a very low minimum near the outer limit of the solid-body-type core. The fluctuations of the light-beam deflection angle shed some light on the nature of transient phenomena occurring in the vortex. In addition to acoustic resonance, considerable irregular density fluctuations were observed, especially at radii smaller than that of the exhaust opening. This is believed to be because of the existence of periodic fluctuations in the rotational speed of the vortex.

1. Introduction

IN recent years, vortex chambers have been subject to lively interest because of their promise as combustion chambers for rockets and as separators of very fine aerosol particles. In particular, it became evident in various investigations[1–3] that the flow in conventionally designed chambers is strongly affected by the radial inflow that occurs in the end-wall boundary layers. Therefore, the structure of such vortices differs considerably from that of free vortices (e.g., the wing-tip vortex of an airplane).

The present investigation is concerned with an air vortex in a swirl chamber of the "reversed-boundary-layer-flow" type. In such chambers, the detrimental radial leakage through the end-wall boundary layers is suppressed by using twin chambers of suitable wall contour and distributing the inlet nozzles so that part of the fluid is being admitted at the end-walls. As a result, the radial flow velocities and the rotating speed of the vortex are more uniform in the axial direction than in conventional chambers. Consequently, the structure of the flow is likely to resemble free vortices much more closely.

It was felt, therefore, that insight into the structure of the flow in the present chamber might be of basic interest apart from the practical interest associated with the application of the chamber for separating a condensible vapor from a carrier gas. The aim was to study the undisturbed conditions in the vortex (as contrary to the conditions when the vortex is "spoiled" by pressure probes). Since the chambers were normally operated at high-inlet pressures ($\gtrsim$100 psig), compressibility effects were pronounced, and this permitted the application of optical density-measuring techniques.

The present chamber belongs to a class of swirl chambers designed by von Ohain[4] and used for particle and vapor separation purposes. Its excellent separation capabilities (reaching down to water droplet sizes of 0.3 μ diam) have been reported earlier by Fletcher et al.[5] Basic aerodynamic studies, using wall taps, a diametral pressure probe, and an anemometer have been performed on similar chambers by Pinchak and Poplawski.[6] In these studies, however, the vortex was affected in an uncontrolled manner by the measuring probes, and probe failure prohibited some measurements. Nevertheless, it became apparent that the peak tangential velocity may be very high (tangential Mach number of about 1.4) and that the rotational speed of the vortex core may be as high as one million rpm.

Looking at the vortex in a transparent (plexiglass) chamber during the start-up or shut-down period revealed that perceptible optical-lens effects were present in the vortex core. This observation gave the impetus to developing the present method. This method falls into the category of "deflection-mapping" methods used in experiments on flames. The deflection of a thin light beam traversing the vortex in a plane perpendicular to the chamber axis is measured for various off-axis positions of the beam. From the deflection-angle distribution, the radial variation of air density can be calculated.

It should be noted that the use of interferometric methods was out of question for at least three reasons. 1) Uninterrupted viewing of at least one half of the chamber diameter

Presented as Paper 68-694 at the AIAA Fluid and Plasma Dynamics Conference, Los Angeles, Calif., June 24–26, 1968; submitted September 20, 1968; revision received April 23, 1969. This work was performed at the Aerospace Research Laboratories of the United States Air Force Office of Aerospace Research, at Wright-Patterson Air Force Base, Ohio, as part of an in-house research program. Reproduction in full or in part is permitted for any use of the U.S. Government. The author takes pleasure in expressing his thanks to H. J. P. von Ohain and to Wolfgang Braun for their encouragement and for helpful discussions on the subject. W. Neely and P. Skinner are thanked for carrying out the numerical calculations and for assisting in the measurements, respectively.

* Staff Research Engineer, Fluid Dynamics Laboratory (Dept. TFVL). Formerly, Research Scientist at the Aerospace Research Laboratories, Wright-Patterson Air Force Base, Ohio. Member AIAA.

would have been required; however, large pressure forces and the possibility of reflections discouraged the use of delicate ring-shaped windows. 2) Such windows would have been difficult to obtain in the required high optical quality, not to mention costs. 3) It was felt that the deflection-mapping method would have a higher accuracy than methods based on the evaluation of interference fringes.

Besides merely allowing disturbance-free measurements, the optical method has some further advantages over conventional ones. It allows us, e.g., to survey the influence of any given pressure probe on the vortex; this, in turn, permits us to make corrections for the probe readings, and enhances the credibility of pressure distributions. Also, the optical instrumentation is of extremely fast response and allows registration of transient phenomena occurring in the interior of the vortex.

One might finally add that the present optical method seems to be inherently better suited for the observation of large objects (e.g., tornadoes). In case of small objects (like the present swirl chamber), good radial resolution requires the use of extremely thin (~0.5 mm) light beams. Then, however, diffraction effects tend to blur out the beam and thereby reduce the sensitivity of the method.

2. Relationship between Light-Beam Deflection and Density Profile

Basic Equations

Three assumptions will constitute the basis for the following theoretical considerations: 1) that the swirl chamber has a circular cross section and the density field is rotationally symmetric; 2) that the density field is axially uniform so that the beams in a plane perpendicular to the chamber axis remain in this plane; and 3) that the deflection is so small that the deflected beam may still be regarded as a straight line. Assumptions 2 and 3 are well fulfilled; assumption 1 is not quite fulfilled in the proximity of the wall, because of the flat windows used that lead to a polyhedral wall contour in the optical planes (cf. Sec. 3).

If a light beam B, see the left half of Fig. 1, traverses a medium in which the refractive index n is a function of radial coordinate r, the beam becomes curvilinear, its angular deflection $d\beta$ over a path dy being given by the Snellius-Descartes law as

$$d\beta = |\text{grad } n| \sin\alpha dy \tag{1}$$

where $\sin\alpha = \cos\varphi = x/r$, x being the lateral and r the radial coordinate of the path element. The sense of $d\beta$ is such that the beam is deflected toward regions of higher density.

Refractive index and density ρ of air are coupled by the equation

$$n - 1 = (n_0 - 1)\rho/\rho_0 \tag{2}$$

where subscript 0 refers to standard conditions. For red light of $\lambda = 6328$ Å, n_0 of air has the value $n_0 = 1.00027661$ (p_0 and T_0 are taken 760 mm Hg and 15°C, respectively). At the densities of concern, n differs only slightly from unity and therefore $d\beta/dy$ remains very small (typically of the order of 10^{-4} rads/cm or smaller).

A light beam entering the circular flowfield at a position x covers a path of $2(r_w^2 - x^2)^{1/2}$ within the vortex (r_w is the radius of the chamber wall). Its total deflection will be

$$\beta(x) = 2\int_0^{(r_w^2-x^2)^{\frac{1}{2}}} \frac{d\beta}{dy} dy = 2\frac{n_0 - 1}{\rho_0}\int_0^{(r_w^2-x^2)^{\frac{1}{2}}} \frac{d\beta}{dr} \times \cos\varphi dy \tag{3}$$

If the deflection angle distribution $\beta(x)$ is known from measurement, the determination of the density profile $\rho(r)$ involves the solution of an integral equation. Equation (3) may be shown to be of Abel's type. The solution is best carried out numerically.

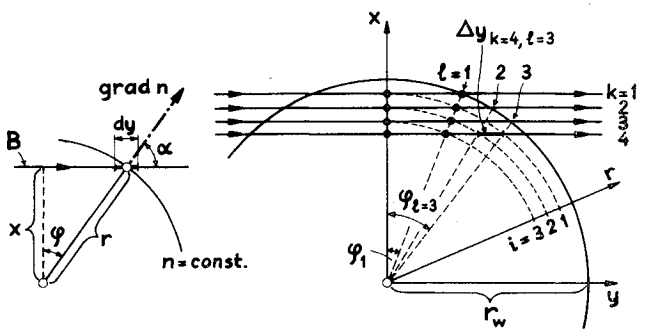

Fig. 1 Illustration of the relationship between density field and light deflection.

Numerical Solution

There are a large number of numerical procedures for solving Abel's integral equation. In view of the great accuracy required in the present case, a slightly different approach has been devised[7] which permits the use of a very fine mesh without causing excessive computer times. The basic point is to use a mesh (see the right half of Fig. 1) which is composed of light beams $k = 1, 2, 3, 4, \ldots$ unequidistantly spaced according to the relation

$$x_k = C^k r_w \quad (k = 1,2,3,\ldots) \tag{4}$$

and of circles $i = 1, 2, 3, \ldots$ having radii according to

$$r_i = C^i r_w \quad (i = 1,2,3,\ldots) \tag{5}$$

the beams and circles intersect at rays $l = 1, 2, 3, \ldots$ which are inclined to the x axis under angles φ_l such that

$$\cos\varphi_l = C^l \tag{6}$$

At the intersection of the kth beam with the ith circle, the ray index has the value $l = k - i$. The value of the constant C is chosen to be slightly smaller than one (e.g., $C = 0.998$).

Equation (3) may now be written in finite-element form, by composing each beam of sections $\Delta y_{k,l}$ ($l = 1, 2, \ldots, k$) as indicated in Fig. 1. The resulting equation for the kth beam is

$$\beta_k = 2\frac{n_0 - 1}{\rho_0}\sum_{l=1}^{k}\left(\frac{d\hat{\rho}}{dr}\cos\varphi\right)_{k,l}\Delta y_{k,l} \tag{7}$$

where $\hat{\rho} = \rho - \rho_w$ has been introduced for convenience in lieu of ρ (ρ_w is the density at the wall). Approximating the expression in parentheses by using the $\hat{\rho}$, r, and φ values pertaining to adjacent meshpoints, one obtains

$$\beta_k = 2\frac{n_0 - 1}{\rho_0}\sum_{l=1}^{k}(\hat{\rho}_{k-l} - \hat{\rho}_{k-l+1})F_l \tag{8}$$

where the notation $\hat{\rho}_i$ is equivalent to $\hat{\rho}(r_i)$ and

$$F_l = K\frac{\cos\varphi_{l-1}\cos\varphi_l}{\cos\varphi_{l-1} - \cos\varphi_l}\frac{\cot\varphi_{l-1} - \cot\varphi_l}{\cot\varphi_{l-1}\cot\varphi_l} \tag{9}$$

The coefficient K has the value $\cos\varphi_{l-1}$ or as $\cos\varphi_l$ depending on the approximation adopted for φ; actually, solutions were computed both ways and the final solution was taken as their arithmetic mean. Equation (8) in fact represents a system of an infinite number of equations for $k = 1, 2, 3, \ldots$ by which the values $\hat{\rho}_{i=k}$ are successively determined for $k = 1, 2, 3, \ldots$ From these equations, making use of the relation $\hat{\rho}_{i=k=0} = \hat{\rho}(r_w) = 0$, the expression

$$\hat{\rho}(r_k) = \frac{1}{F_1}\left[-\frac{\beta_k}{2}\frac{\rho_0}{n_0 - 1} + \sum_{n=1}^{k-1}(F_n - F_{n+1})\hat{\rho}_{k-n}\right] \tag{10}$$

is obtained, which permits the successive calculation of $\hat{\rho}(r_k)$ for $k = 1, 2, 3, \ldots$

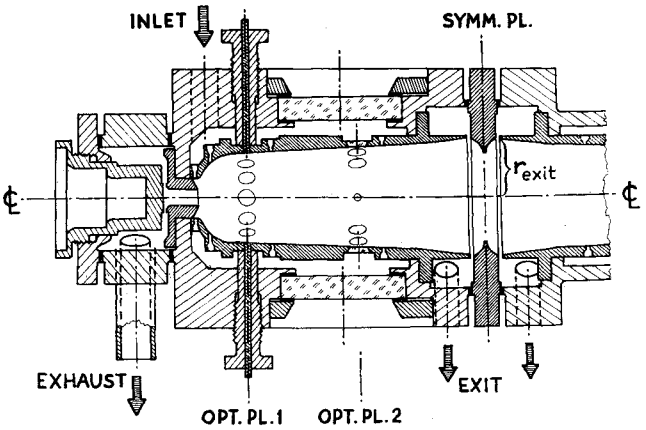

Fig. 2 Cut-away view of the swirl chamber (only the left half is shown).

The computer program dealing with this procedure is described in Ref. 7 in detail. In a test case, it has been found to lead to errors which are by an order of magnitude smaller than the errors of a program which was based on a procedure[8] used as a standard one in similar studies.

3. Apparatus

Swirl Chamber

General description

The chamber is operated with dry air of approximately room temperature. The inlet pressure may be set at any desired value in the range 0–400 psig. The vortex is created in an elongated, approximately cylindrical cavity consisting of two symmetrical halves and formed by a pair of stainless-steel inner housings. These resemble the shape of a bell and intercommunicate at their open ends. The longitudinal cross section of the left chamber half is shown in Fig. 2. The total length of the cavity is 18 in.; its largest diameter is $2r_{exit} = 3.63$ in.

The "bells" are accommodated in an outer housing, which leaves a mantle space around the bells. The inlet air first enters this space and is then injected through a number of tangential nozzles of $\frac{1}{16}$ in. diam into the chamber. In eight rows, a total of 48 nozzles is provided. The rows are distributed along the chamber contour in accordance with the desire to counteract the influence of the end-wall boundary layers.

The air leaves the chamber in two different streams: the "exhaust" flow (a low-pressure, high-speed, whirling flow) leaves axially at both ends of the chamber through round exhaust ports having a diameter of $2r_{exh} = 0.50$ in.; before being discharged to the atmosphere, the exhaust flow passes at both ends through a narrow radial diffuser provided just outside the exhaust port. These diffusers serve several purposes: they prohibit the sucking-in of atmospheric air along the vortex centerline, permit creation of vacuum pressures along the centerline, and allow variation of the amount of exhaust flow by adjusting the diffuser gap width. This latter was of the order of $\frac{1}{32}$ to $\frac{1}{8}$ in. and was adjusted so that always the greatest possible vacuum at the centerline was obtained.

The rest of the flow leaves as a high-pressure low-speed stream, called the "exit" flow, through circumferential slots provided between the bell edges and the flange located in the middle of the chamber. The exit flow is discharged through a throttle valve to the atmosphere; by adjusting this valve, the pressure level in the exit manifolds, i.e., the amount of exit flow, can be varied. In the operating condition most frequently used, about half of the inlet mass flow was taken out through the exit.

Instrumentation

Optical measurements can be made in two cross sections of the chamber (optical planes No. 1 and No. 2, see Fig. 2) where two circumferential rows of small, circular, closely spaced quartz windows are provided in the bell. In the outer housing, large windows allow light to pass through various pairs of bell windows. In Fig. 2, the light beam used in Opt. Pl. 1 is perpendicular to the plane of the drawing; in Opt. Pl. 2, the beam is parallel to the drawing. (The chamber has to be tilted 90° when changing from one optical plane to the other.) The pieces of metal separating the adjacent windows cover certain radial ranges within the vortex; however, by slightly tilting the chamber with respect to the light beam, these ranges can be uncovered and thereby the distribution of the deflection angle can be mapped uninerruptedly.

In each optical plane, a pair of probe holes is provided, the hole axis being perpendicular to the direction of light. In Fig. 2, the holes in Opt. Pl. 1 are seen to be plugged up by solid rods. Other plugs, equipped with a thermocouple or a static-pressure tap, were used to measure temperature and pressure at the vortex periphery in combination with the optical measurements. The relative position of the light beam with respect to the chamber centerline could be checked and calibrated (while the chamber was not in operation) with help of special rods inserted through these probe holes.

Additional, conventional instrumentation included wall taps for pressure distribution measurements in the region of the exhaust ports (including the conical front face of the insert comprising the exhaust port, the cylindrical wall of the port, and the face of the exhaust diffuser cap), axial pressure and temperature probes which were able to scan along the centerline within the exhaust ports, and a radial static-pressure probe inserted at the symmetry plane. This latter probe markedly disturbed the vortex if it penetrated deep into the

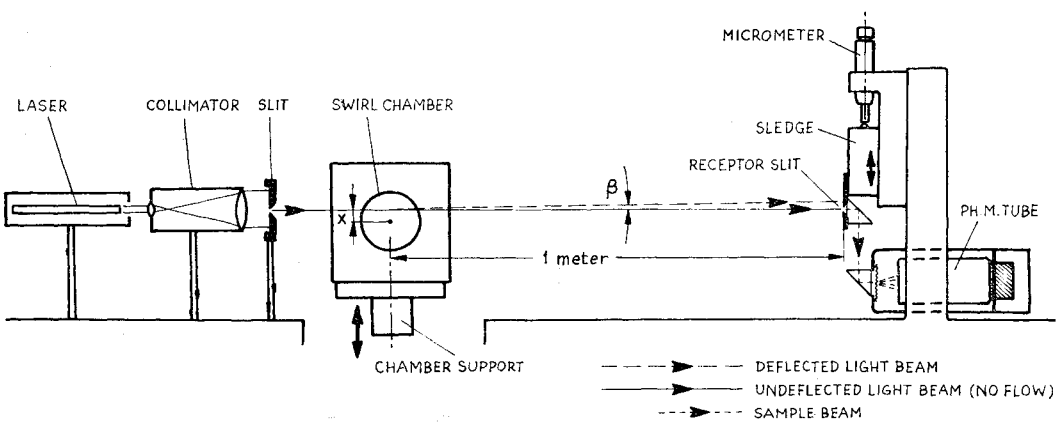

Fig. 3 Schematic drawing of the optical set-up.

flow, and therefore optical measurements of the density profile were carried out at various probe penetrations in order to have a basis for correcting the probe readings.[7]

Optical Set-up

The scheme of the optical apparatus is shown in Fig. 3. Although the optical components are rigidly mounted on a large I-beam, the chamber is supported by a vertically movable platform that is mounted on a milling-machine table. Once the relative position of the light beam with respect to the chamber axis x (see Fig. 3) has been calibrated, the milling-machine's vertical adjustment permits precise setting of x at any desired value.

To the left of the chamber, a slit is used to cut out a thin light beam from the expanded parallel light bundle produced by a laser/collimator system. (Coherent light is not required for the measurements, but arc-lamp sources were discarded because of their irregular intensity fluctuations.) The light beam has a vertical width of 0.6 mm and a horizontal width of 4 mm at the beam-cutting slit. At the receptor unit, i.e., about one meter farther away, the vertical width of the beam increases to about 0.8 mm as a result of diffraction. (Here, the vertical intensity profile of the beam already has assumed a Gaussian-like shape, and the width of 0.8 mm refers to the half-intensity points.)

One meter behind the axis of the chamber, a receptor unit is mounted in order to measure the deflection of the light beam. This unit comprises a very thin (~0.025 mm) slit and a photo-multiplier tube mounted behind the slit. The slit can be moved in the vertical sense by using a micrometer spindle. The photo-multiplier measures the intensity of light passing through the receptor slit (sample beam). Care is taken that the photocathode area used should not change if the receptor slit is being displaced. By moving the receptor slit across the light beam, the vertical intensity profile of the beam may be measured by measuring the photo-current of the tube.

In the actual measurements aimed at determining the time-mean deflections caused by the vortex, the position of the light beam was measured in a very simple way. Instead of letting the beam impinge directly on to the slit, a beam wobbler (a glass plate of $\frac{1}{4}$ in. thickness mounted on a horizontal shaft) was placed at a short distance in front of the slit. The glass plate could be wobbled between two tilted positions that were inclined by equal angles to the vertical (neutral) position. As a result, the beam at the slit was moved upward or downward from its undisturbed position. The receptor slit was then merely used to find the point where the intensity was the same for both cases, i.e., the point where the two shifted Gaussians intersected; this point indicated the center of the undisturbed beam.

In each experiment, the location of the light-beam center was determined first without flow for a number of beam positions x; then the chamber was put into operation at the desired operating condition, and the measurement was repeated for the same x positions. The difference in the vertical position of the beam center at the receptor plane without and with flow gives the total deflection of the light beam for the x value in question. This total deflection is, however, only partly due to the density field of the vortex itself; an important part is caused by refraction effects associated with merely raising the pressure level at the vortex periphery and in the mantle space surrounding the bell to the particular values required for operating the chamber. The magnitude of these parasitic refraction effects is calculated by a computer program (on the basis of the geometric data of the windows and the value of air density at the vortex periphery and in the mantle space) for each measured point and is subtracted from the total deflection. The result gives the net deflection $\beta(x)$ caused by the density field inside the vortex.

Typically, the total deflection causes a vertical shift of about 0 to 2 mm at 1 meter distance, i.e., it is of the order of 0 to 2 $\times$ 10^{-3} rads. The corrections due to parasitic effects are very small (~0.01 mm) at small x/r_w values; at about $x/r_w = 0.4$ they become of the same order as β. It is estimated that the final accuracy of the β values lies within 2×10^{-5} rads. The results of such measurements will be shown in the upper part of Fig. 4.

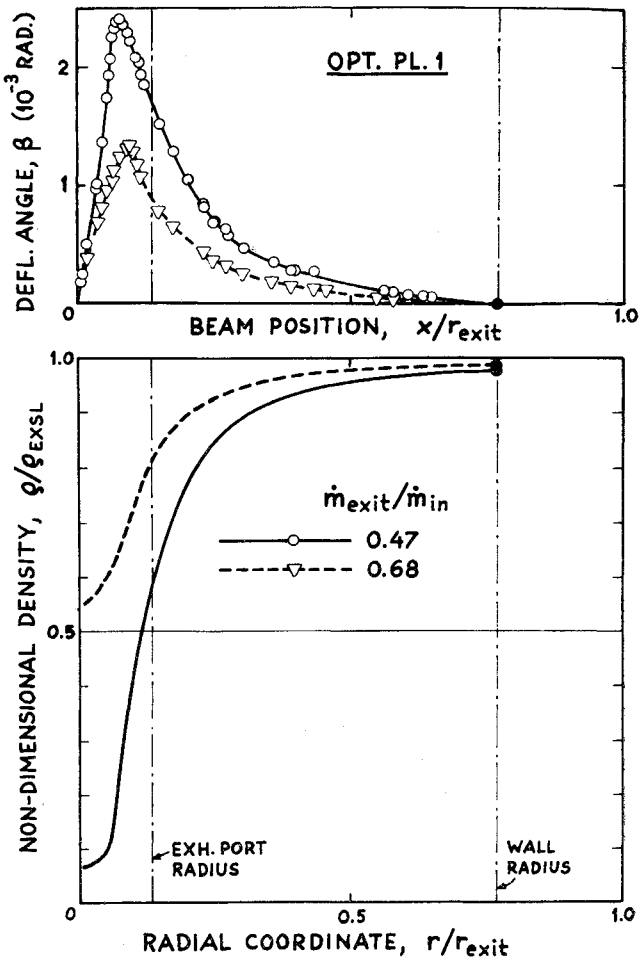

Fig. 4 Measured deflection-angle distributions and calculated density profiles in Optical Plane No. 1, for two different operating conditions.

For the measurements aimed at observing the fluctuations of β with time, the procedure was different: The flow was turned on and the chamber was set at some position x; the receptor slit was moved into the place where the Gaussian intensity profile of the beam had its steepest gradient, and was left there. Now if fluctuations of the beam deflection occurred, the Gaussian moved up and down in the receptor plane and there was a variation in the intensity of the sample beam. The fluctuations were made visible by connecting the photo-multiplier output to an oscilloscope. The vertical scale of the oscillograms could be directly calibrated in terms of deflection angle by keeping the beam stationary (no flow) and moving the slit. Oscillograms obtained this way will be shown later in Fig. 7. A more detailed description of the apparatus is available in Ref. 7.

4. Results of Time-Mean-Measurements

Operating Conditions

From the various conditions investigated,[7] two typical ones will be discussed in the present paper. In both conditions, the pressure and temperature of the air in the inlet mantle space are the same (p_{in} = 114.7 psia = 7.91 bar, T_{in} = 59°F = 288°K), but the exit-flow ratio (i.e., the ratio of exit

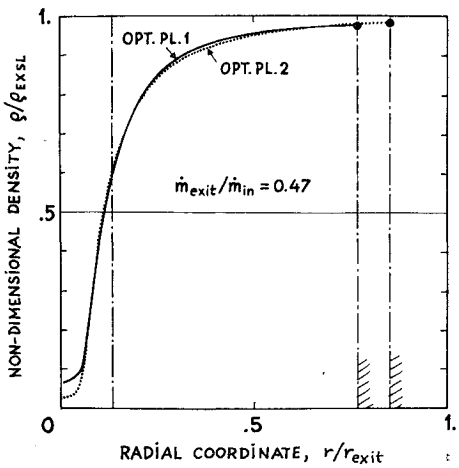

Fig. 5 Density profile in the two optical planes (at the same operating condition).

mass flow rate to inlet mass flow rate) differs, having the values $\dot{m}_{exit}/\dot{m}_{in} = 0.47$ and 0.68, respectively.

In plotting the results, the data will be referred to the values existing at the largest radius in the vortex which is the radius at the exit slots (r_{exit} = 1.81 in. = 46 mm). The pressure and temperature at the exit slot have the values p_{EXSL} = 84.7 psia = 5.84 bar, T_{EXSL} = 74°F = 296°K at the exit-flow ratio of 0.47, and the values p_{EXSL} = 98.3 psia = 6.78 bar, T_{EXSL} = 65°F = 291°K at the exit-flow ratio of 0.68.

The centerline pressure measured at the exhaust diffuser face was found to have the values $p_{EDF-0} \approx 7.7$ psia = 0.53 bar and 44 psia = 3.04 bar, respectively. This strong difference indicates that the intensity of the vortex is greatly reduced in the present chamber if more than half of the inlet flow is allowed to pass through the exit rather than through the exhausts.

Results for Two Different Exit-Flow Ratios

Figure 4 shows the results of the density measurement made in Optical Plane 1 for the two operating conditions mentioned above. In the upper part of the figure, the distribution of the deflection angle β is plotted over the beam position, the latter being made nondimensional with the help of r_{exit}. The vertical dash-and-dot lines mark the radius of the exhaust ports (r_{exh}/r_{exit} = 0.25″/1.83″ = 0.138) and of the wall in Optical Plane 1 (note the slightly conical shape of the chamber, shown in Fig. 2).

It is seen that the deflection angle distribution has a sharp peak at a radius lying well inside the radius of the exhaust ports. This is associated with the steep density gradient occurring in this zone. The deflection angle is zero at $x = 0$, as required by symmetry, and tends toward zero (black dot) as x approaches the wall. The bell windows did not allow the light beam to pass closer to the wall than indicated by the last data point. It is seen that the light deflections are greater if the vortex is more intense (exit-flow ratio 0.47). The data points define a continuous curve $\beta(x)$ that can be fed into the computer program and used, together with the density value at the wall, to evaluate the density distribution in the vortex according to the numerical procedures described in Sec. 2.

The resulting density profiles are plotted in the lower half of Fig. 4. It is seen that more than half of the drop in density occurs inside the radius of the exhaust ports; the parabola-like portion in the density profile—which corresponds to the well-known parabolic pressure profile associated with solid-body-type rotation—is seen to be limited to the innermost region of the vortex and to extend only to a radius of about half of the exhaust port radius. The density in the center of the vortex is greatly different for the two operating conditions; this complies with the difference observed in the pressure measurements made at the center of the exhaust diffuser caps. (It should be noted, though, that the pressure in Optical Plane 1 actually turns out to be lower than at the diffuser caps and to decrease further toward the symmetry plane.)

Comparison of Two Cross Sections

Earlier investigations[5] made with a swirl chamber of the same geometry involved experiments with humid air (in which case a condensation cloud surrounding the axis of the vortex was found to appear), used tracing water on the chamber walls, and included a detailed probe study of the flow structure within the exhaust ports. These investigations revealed that the vortex had nearly uniform intensity throughout the length of the chamber. Regarding the meridional flow pattern existing in the chamber, they showed that the velocity near the bell wall had a slight axial component pointing toward the symmetry plane, that there was a fast-rotating, high-axial-speed flow directed toward the exhaust ports in the annulus lying between the radii $r \approx 0.4\, r_{exh}$ and $r \approx r_{exh}$′ and that there was no appreciable axial outflow through the exhaust ports at radii smaller than about $0.4\, r_{exh}$ (evidence rather suggested a back-flow into the chamber). In the exhaust ports, the highest value of the tangential Mach number M_t was found to be about 1.4 and the highest value of the axial Mach number M_z to be about 1.2.

The present measurements yielded the density profile in the two cross sections shown in Fig. 2. Typical results (with an exit-flow ratio of 0.47) are shown in Fig. 5. It is seen that the two density profiles are very much alike. In the outer parts of the vortex (at $r/r_{exit} > 0.2$) the density is seen to be slightly higher in Opt. Pl. 1 than in Opt. Pl. 2; this indicates an axial pressure gradient which might be the reason for the flow toward the symmetry plane observed in earlier investigations. In the range $0.08 < r/r_{exit} < 0.2$, which roughly corresponds to the zone of high-axial-speed flow, the density—and, most likely, the pressure—are lower in Opt. Pl. 1 than in Opt. Pl. 2. This indicates an axial pressure decrease toward the exhaust ports. However, this axial pressure gradient is too small to explain the acceleration of a fluid particle to the high (locally even supersonic) axial Mach numbers existing in the exhaust port. It must be assumed, therefore, that the meridional streamlines in the high-axial-speed zone, though almost parallel to the centerline, converge toward the exhausts. Finally, in the innermost zone of the vortex ($r < 0.4\, r_{exh}$), there again is seen a density (and pressure) increase toward the exhaust ports. The lowest density (and pressure) is found to occur at the symmetry plane rather than in the exhausts. This phenomenon is probably because of the two

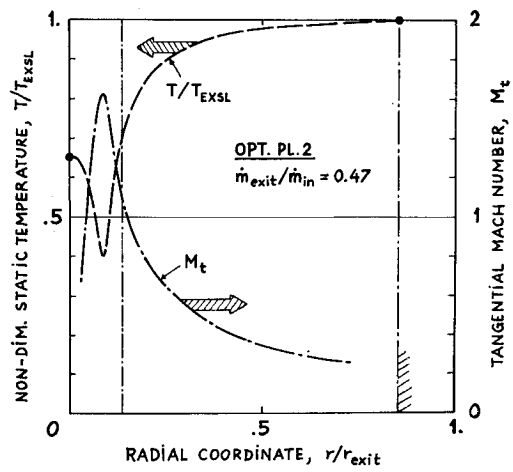

Fig. 6 Profiles of static temperature and tangential Mach number.

high-axial-speed annular streams directed at the exhaust ports acting as ejectors and creating a high vacuum in the middle portion of the vortex core.

Static-Temperature Profile

The static-temperature profile in the middle portion of the vortex can be inferred from the density profile in Opt. Pl. 2 and the static-pressure profile at the symmetry plane. The latter has been measured with a probe radially inserted into the vortex. Thanks to parallel observations of the density profile in Opt. Pl. 2, the disturbances created by the probe could be checked and the probe readings could be corrected to give a reasonably reliable pressure distribution down to a radius of $r/r_{exit} = 0.10$. Thermocouple surveys along the centerline in the vicinity of the exhaust ports indicate that the centerline static temperature assumes a constant value $T_{\mathfrak{C}}$ inside the chambers, which has the value 0.65 T_{EXSL} in the operating condition in question. It may further be assumed that the radial profiles of pressure and density undergo only negligible changes between Opt. Pl. 2 and the symmetry plane. (Because fast changes in the profiles are more likely to occur near the exhausts than around the symmetry plane; however, the changes actually found are slight between the two optical planes and slight even between Opt. Pl. 1 and the end-wall.) With this assumption and with the known value of $T_{\mathfrak{C}}$ it is possible to infer the centerline value of pressure from the centerline density in Opt. Pl. 2; with the centerline pressure in hand, the missing part of the pressure curve (covering the range $0 < r/r_{exit} < 0.10$), which is known to have a roughly parabolic form, can be reasonably well estimated. Then, the density and pressure profiles are complete, and—bearing in mind the previous assumption—they may be used to calculate the static-temperature profile in the middle of the vortex.

The result is shown in Fig. 6 by the dashed curve. It is seen that the static temperature has a very low minimum (of about $T_{min} = 0.4\ T_{EXSL}$!) in the zone where the steepest density gradients occur (cf. Fig. 5). The error in the absolute value of T_{min} may be as high as $\pm 20\%$ (as a result of the uncertainties inherent in the way T_{min} has been inferred), but there is no reason to doubt the existence of a minimum that is outside the core of the vortex.

One would expect generally to find the lowest static temperature at the axis of the vortex; maybe the reason for the present anomalous finding is a radial leakage that occurs in the boundary layer of the exhaust diffuser caps and which fills the vortex core with relatively warm air.

Tangential Mach Number Profile

According to Pinchak,[9] the tangential Mach number in rotationally symmetric, turbulent or laminar, viscous or nonviscous flow, in which the axial and radial velocities are small compared to the tangential one, can be calculated directly from the radial static-pressure profile $p(r)$ using the relation

$$M_t = [(r/\gamma p)\ (dp/dr)]^{1/2} \tag{11}$$

where γ is the isentropic exponent of the medium. The Mach number distribution calculated in this manner from the pressure profile at the symmetry plane is shown in Fig. 6 (dash-and-dot curve).

The M_t curve shows that the highest tangential velocities are reached at a radius much smaller than the radius of the exhaust ports. The peak M_t value at the symmetry plane is considerably supersonic ($\sim$1.6), i.e., similarly high as the peak found within the exhaust ports.[5] Inside the M_t-peak, the air rotates like a solid body, and the rotational speed inferred from the slope of the M_t curve is 1×10^6 rpm. Outside the peak, M_t falls off in a way resembling the hyperbolic tangential-velocity variation in potential flow.

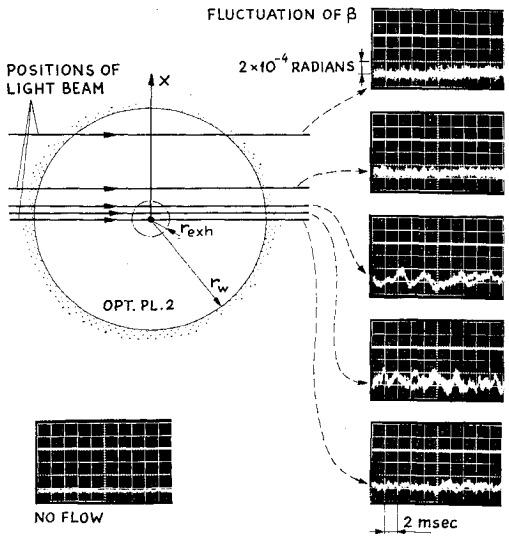

Fig. 7 Fluctuation of the deflection angle β at various beam positions.

5. Observation of Transient Phenomena

As described in Sec. 3, it was possible to display the fluctuations of the deflection angle on the screen of an oscilloscope. Results obtained at five different positions of the light beam with respect to the vortex axis are shown in Fig. 7. (The operating conditions are the same as in Figs. 5 and 6; the recording was made in Optical Plane 2.)

If the five oscillograms obtained with flow are compared to the oscillogram that shows the trace without flow, two distinct kinds of fluctuation can be recognized: One is an irregular, relatively slow fluctuation (lying roughly in the frequency range 300–500 cps) which is very pronounced for the two beams crossing the projected area of the exhaust port at some distance from the axis and also is present, to a smaller extent, in the beam crossing the axis; it is absent, however, at the larger radii. The other fluctuation has a much higher frequency ($\sim 10^4$ cps) and can be shown to have a very regular sine-type character. At the time scale of the oscillograms shown in Fig. 7 (1 cm = 2 msec), these fast fluctuations only appear as a blur of the traces.

Although the fast fluctuations seem to be attributable to acoustic resonance in the chamber, it is interesting to speculate about the nature of the irregular, slow fluctuations. For sake of discussion, the root-mean-square amplitude of these slow fluctuations, $\overline{\Delta\beta}$, has been determined from oscillograms for a number of beam positions and superposed on the time-mean distribution of the deflection angle, see the upper curve in Fig. 8. (The fluctuations are exaggerated in the figure.)

In an attempt to interpret these fluctuations, one has to bear in mind that the $\overline{\Delta\beta}$ value observed at any beam position is a summed-up result of various influences suffered by the beam along its path. The interpretation is simple if $\overline{\Delta\beta}$ becomes larger as the beam is moved closer to the center: in this case a zone of stronger flow fluctuations must have been touched upon by the beam. However, if $\overline{\Delta\beta}$ happens to decrease, there are several possible explanations: e.g., the newly reached inner zone may have flow fluctuations that tend to cancel the effect of the outer zones; or, the effect of the outer zones may be fading out by geometric reasons, whereas the inner region is free of fluctuations. [This could be possible, for example, if the $\overline{\Delta\beta}$ originating in an outer zone were caused mainly by variations in the radial (not the tangential) component of grad ρ; then the factor $\sin\alpha$ in Eq. (1) would cause a decrease of $\overline{\Delta\beta}$ as the beam is moved toward the center.] Further, it has to be remembered that the various oscillograms have been recorded at various times. Therefore

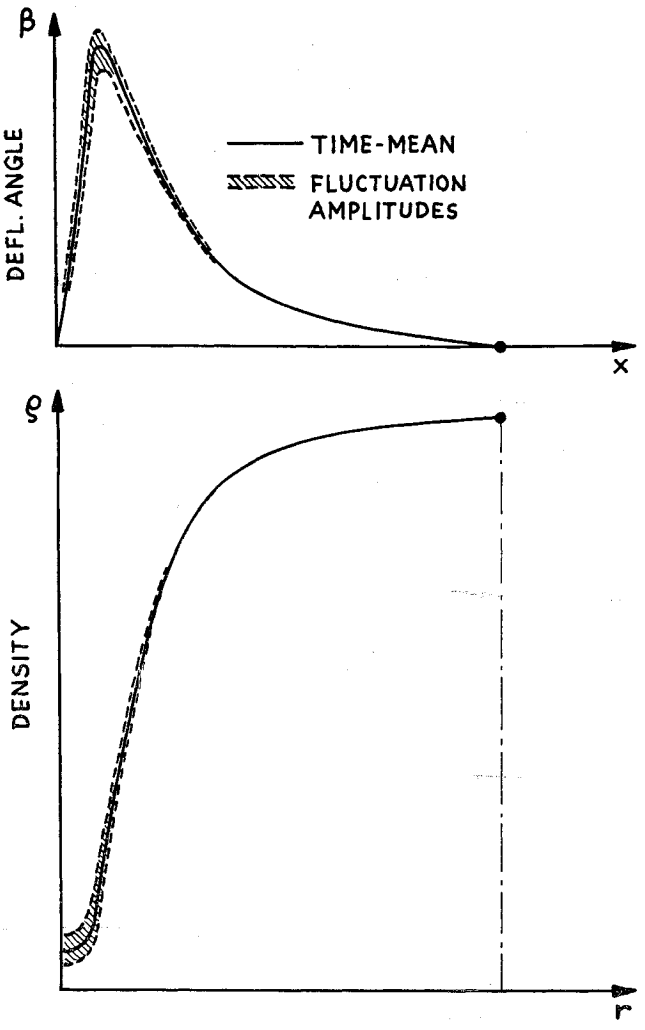

Fig. 8 Interpretation of the deflection-angle fluctuations.

it is not known whether a certain fluctuation observed at a particular beam position is coupled with similar simultaneous fluctuations at other beam positions.

It is easy to identify some types of flow fluctuations that cannot explain the observed $\overline{\Delta\beta}$ distribution. An erring around the vortex axis near the chamber centerline would shift the $\beta(x)$ curve to and fro in the x direction and therefore cause significant $\overline{\Delta\beta}$ values only at the steep portions of the $\beta(x)$ curve.

A pulsation of the diameter of the viscous core of the vortex without significant changes in the peak tangential velocity would leave the peak value of β practically constant and would merely shift its position in the x direction. This also contradicts the observed large fluctuations of β in the peak region.

Core diameter pulsations caused by an oscillation of the point of transition from the potential-type vortex to solid-body-type rotation would result in $\overline{\Delta\beta} = 0$ outside the range of oscillation, whereas $\overline{\Delta\beta}$ would increase abruptly within this range. No such abrupt increase of $\overline{\Delta\beta}$ toward lower x values has been found experimentally.

Very strong turbulence limited to the zone where the maximum $\overline{\Delta\beta}$ values are found would not explain the near disappearance of $\overline{\Delta\beta}$ for $x = 0$, because turbulence would cause fluctuating tangential density gradients as well as fluctuations in the radial density gradient (no sinα-effect). The following two hypotheses may be conceived which do not contradict the observed $\overline{\Delta\beta}$ distribution.

First, the existence of pronounced turbulence throughout the inner region of the vortex, causing strong fluctuations in beams passing near the periphery of the turbulent region and causing weaker fluctuations in beams passing near the axis (because of cancellation by averaging out). However, this explanation, although possible, is made rather unlikely because any local beam deflection caused is, among other factors, proportional to the absolute magnitude of density; therefore, the level of turbulence (meaning here the percentage-wise fluctuation of density) ought to be the highest in the core where the density is the lowest in order to be able to cancel out the effect of the higher-density turbulent zones lying farther outside. However, it is doubtful whether turbulence exists at all in the viscous core, not to speak of its level being the highest.

Second, irregular variations in the rotational speed of the inner regions of the vortex, including both the viscous core and at least the adjacent portions of the potential-type vortex. Namely, the observed $\overline{\Delta\beta}$ distribution has the remarkable feature that $\overline{\Delta\beta}$ is almost exactly proportional to β. A simple explanation for this is that the radial density gradient simultaneously increases or decreases throughout the vortex, causing a vacillation of the density profile between some upper and lower extremes, as sketched in the lower half of Fig. 8. Such density profile changes presuppose, of course, variations in the rotational speed of the vortex. The measured values of $\overline{\Delta\beta}$ indicate that these speed fluctuations ought to be of the order of 3–5%.

This explanation is supported by the fact that the pressure at the centerline of the vortex showed irregular variations that often made manometer readings rather difficult. Unfortunately, there was no possibility to check whether the fluctuations at various beam positions occurred simultaneously, because the one-beam optical apparatus could not be modified into a two-beam one within the time available for these experiments. Therefore, the possibility cannot be dismissed with certitude that there is still another explanation for the observed fluctuations which has not been thought about here.

6. Conclusions

Light-beam deflection-mapping proved to be a useful method for gaining additional insight into the flow phenomena occurring in a vortex. Remarkable features of this method are its great accuracy, the fact that the vortex is not disturbed by probes, and the possibility of observing transient phenomena.

In order that this method may be applied, compressibility effects have to have a certain magnitude. This was insured in the present vortex chamber where the air pressure decreased from about 80 psia near the wall to a few psia at the vortex axis.

From the optically measured density profiles and from the results of routine pressure and temperature measurements, the following conclusions may be drawn:

1) As expected in a swirl chamber where end-wall boundary-layer inflow is suppressed, the density profiles turn out to be almost identical in various cross sections of the vortex. Their slight differences allow delineation of zones where the direction of axial flow varies.

2) From the slight magnitude of axial density gradients in the zone where the high-axial-speed exhaust flow is formed, it can be inferred that meridional streamlines of the exhaust flow continue to approach the axis even after the radial inflow has turned into an essentially axial outflow.

3) The high-speed axial outflow occurring in the zone surrounding the vortex core and directed toward both ends of the chamber creates very low pressures and densities along the middle portion of the vortex axis (ejector effect).

4) The steepest density gradients, the lowest static tem-

peratures, and the highest tangential velocities (Mach number 1.6) occur at a radius that is roughly half of the radius of the exhaust ports.

5) The rotational speed of the vortex core in the present chamber was typically 1 million rpm.

6) The nature of observed light-beam deflection-angle fluctuations suggests that the rotational speed of the vortex is subjected to irregular fluctuations of an amplitude of about 3–5% and of frequencies lying in the range 300–500 cps.

It seems that it would be instructive to observe simultaneously the deflection-angle fluctuations of several light beams crossing the flowfield at various off-axis positions.

References

[1] Rosenzweig, M. L., Lewellen, W. S., and Ross, D. H., "Confined Vortex Flows with Boundary-Layer Interaction," *AIAA Journal*, Vol. 2, No. 12, Dec. 1964, pp. 2127–2134.

[2] Roschke, E. J. and Pivirotto, T. J., "Similarity in Confined Vortex Flows," TR 32-789, Aug. 1965, Jet Propulsion Lab., Pasadena, Calif.

[3] Roschke, E. J., "Flow Visualization Studies of a Confined, Jet-Driven Water Vortex," TR 32-1004, Sept. 1966, Jet Propulsion Lab., Pasadena, Calif.

[4] Hasinger, S. H., Mills, R. H., and von Ohain, H. J. P., Internal Report (restricted circulation), Jan. 1962, Aerospace Research Labs., Wright-Patterson Air Force Base.

[5] Fletcher, E. C., Gyarmathy, G., and Hasinger, S. H., "Separation of Submicron Condensate Particles in a Vortex Chamber," TR ARL-66-0218, Nov. 1966, Aerospace Research Labs., Wright-Patterson Air Force Base.

[6] Poplawski, R. and Pinchak, A. C., "Aerodynamic Performance of Reversed-Flow Vortex Chambers," TR ARL-65-219, Oct. 1965, Aerospace Research Labs., Wright-Patterson Air Force Base.

[7] Gyarmathy, G., "Optical Measurement of Radial Density Distribution in a High-Speed Confined Air Vortex," TR ARL-67-0234, Dec. 1967, Aerospace Research Labs., Wright-Patterson Air Force Base.

[8] Nestor, O. H. and Olsen, H. N., "Numerical Methods for Reducing Line and Surface Probe Data," *SIAM Review*, Vol. 2, No. 10, Oct. 1961, p. 200.

[9] Pinchak, A. C. and Poplawski, R., "On the Attainment of Extremely High Rotational Velocities in a Confined Vortex Flow," AIAA Paper 65-400, San Francisco, Calif., 1965.